Salinity Boundary Conditions and the Atlantic Meridional Overturning Circulation in Depth and Quasi-Isopycnic Coordinate Global Ocean Models

Jianjun Yin[a,*], Eric P. Chassignet[a], William G. Large[b], Nancy J. Norton[b], Alan J. Wallcraft[c] and Stephen G. Yeager[b]

[a]*Center for Ocean-Atmospheric Prediction Studies, Florida State University*

[b]*National Center for Atmospheric Research*

[c]*Naval Research Laboratory, Stennis Space Center*

Revised for *Ocean Modelling*

June 30, 2009

* *Corresponding author address: Jianjun Yin, COAPS, Florida State University, Tallahassee, FL32311 email: yin@coaps.fsu.edu Phone: (850) 644-4174*

Report Documentation Page

Form Approved
OMB No. 0704-0188

1. REPORT DATE	2. REPORT TYPE	3. DATES COVERED
30 JUN 2009		**00-00-2009 to 00-00-2009**

4. TITLE AND SUBTITLE	5a. CONTRACT NUMBER
Salinity Boundary Conditions and the Atlantic Meridional Overturning Circulation in Depth and Quasi-Isopycnic Coordinate Global Ocean Models	5b. GRANT NUMBER
	5c. PROGRAM ELEMENT NUMBER
6. AUTHOR(S)	5d. PROJECT NUMBER
	5e. TASK NUMBER
	5f. WORK UNIT NUMBER
7. PERFORMING ORGANIZATION NAME(S) AND ADDRESS(ES) **Naval Research Laboratory,Stennis Space Center,MS,39529**	8. PERFORMING ORGANIZATION REPORT NUMBER
9. SPONSORING/MONITORING AGENCY NAME(S) AND ADDRESS(ES)	10. SPONSOR/MONITOR'S ACRONYM(S)
	11. SPONSOR/MONITOR'S REPORT NUMBER(S)

12. DISTRIBUTION/AVAILABILITY STATEMENT
Approved for public release; distribution unlimited

13. SUPPLEMENTARY NOTES

14. ABSTRACT

This paper compares the Atlantic Meridional Overturning Circulation (AMOC) in global simulations performed with the depth coordinate Parallel Ocean Program (POP) ocean model and with the HYbrid Coordinate Ocean Model (HYCOM) under different surface salinity boundary conditions. When forced by the Coordinated Ocean-ice Reference Experiment (CORE) repeat Normal Year Forcing, HYCOM develops internal inter-annual variability during the model spin-up, while POP does not and HYCOM is more sensitive to the salinity boundary condition in the Southern Ocean. Otherwise the AMOC and related fields in the two models are qualitatively similar, but neither is able to maintain a non-trivial AMOC, because of a positive feedback that continually freshens the high-latitude surface waters. However, with salinity restoring at the ocean surface the AMOC becomes progressively stronger as the piston velocity is increased. The different restoring strategies in POP and HYCOM cause differences in the AMOC simulation. The components of the AMOC and closely related fields, including the oceanic deep convection, thermohaline fluxes, three dimensional currents, water mass distribution and overflows, are compared between the models with different salinity boundary conditions. The comparison provides insights on the models? response and increases our understanding of ocean climate simulations. It also provides motivation for the future development of ocean climate models capable of simulating the AMOC more realistically.

15. SUBJECT TERMS

16. SECURITY CLASSIFICATION OF:			17. LIMITATION OF ABSTRACT	18. NUMBER OF PAGES	19a. NAME OF RESPONSIBLE PERSON
a. REPORT **unclassified**	b. ABSTRACT **unclassified**	c. THIS PAGE **unclassified**	**Same as Report (SAR)**	**43**	

Abstract

This paper compares the Atlantic Meridional Overturning Circulation (AMOC) in global simulations performed with the depth coordinate Parallel Ocean Program (POP) ocean model and with the HYbrid Coordinate Ocean Model (HYCOM) under different surface salinity boundary conditions. When forced by the Coordinated Ocean-ice Reference Experiment (CORE) repeat Normal Year Forcing, HYCOM develops internal inter-annual variability during the model spin-up, while POP does not and HYCOM is more sensitive to the salinity boundary condition in the Southern Ocean. Otherwise the AMOC and related fields in the two models are qualitatively similar, but neither is able to maintain a non-trivial AMOC, because of a positive feedback that continually freshens the high-latitude surface waters. However, with salinity restoring at the ocean surface the AMOC becomes progressively stronger as the piston velocity is increased. The different restoring strategies in POP and HYCOM cause differences in the AMOC simulation. The components of the AMOC and closely related fields, including the oceanic deep convection, thermohaline fluxes, three dimensional currents, water mass distribution and overflows, are compared between the models with different salinity boundary conditions. The comparison provides insights on the models' response and increases our understanding of ocean climate simulations. It also provides motivation for the future development of ocean climate models capable of simulating the AMOC more realistically**.**

Keywords: Atlantic meridional overturning circulation, global ocean-ice modeling, salinity boundary condition, isopycnic coordinate ocean model, depth coordinate ocean model, circulation stability

1. Introduction

The Atlantic Meridional Overturning Circulation (AMOC) is one of the most important components of the global ocean circulation. The AMOC here refers to the circulation associated with the oceanic deep convection and North Atlantic Deep Water (NADW) formation in the high latitudes of the North Atlantic. A vigorous AMOC in climate models transports a large amount of heat and salt northward in its upper branch, thereby maintaining the high surface temperature and salinity in the northern North Atlantic compared to other oceans at the same latitudes. Failure to represent a strong AMOC would lead to a simulated climate state very different from reality, both in terms of the mean state and in climate variability (Manabe and Stouffer, 1988; Schiller *et al.*, 1997; Vellinga and Wood, 2002; Stouffer *et al.*, 2006).

It is challenging to obtain a realistic AMOC in ocean climate numerical models because the modeled circulation is highly sensitive to the thermohaline forcing at the ocean surface and its equilibration is extremely slow (Rahmstorf, 1997; Griffies *et al.*, 2009). A very small bias in the thermohaline forcing, especially in the freshwater flux, can cause a persistent drift and eventual collapse of the AMOC. One factor is the lack of direct feedback between sea surface salinity (SSS) and the freshwater flux at the ocean surface to control salinity drift. Another factor is a strong positive feedback between the AMOC and northward salt transport in the North Atlantic (Stommel, 1961). A salinity anomaly in the high-latitude North Atlantic induced by the former mechanism can be amplified through the latter, leading to a large salinity drift (Paiva and Chassignet, 2001). In this sense, the AMOC is a relatively unstable system, in contrast to the direct wind-driven circulation. Consequently, uncoupled ocean general circulation models (OGCMs) often require a salinity restoring to introduce a negative feedback to stabilize the AMOC (Griffies *et al.*, 2009). The simulation of the AMOC is more complex in fully coupled

atmosphere-ocean general circulation models (AOGCMs). Despite the lack of salinity restoring, at least some of the AOGCMs that participated in the Fourth Assessment Report (AR4) of IPCC were able to maintain a stable vigorous AMOC in their long-term control runs (Schmittner *et al.*, 2005; Meehl *et al.*, 2007).

Most previous numerical investigations on the AMOC have been performed using depth coordinate ocean models (Bryan, 1986; Stocker and Wright, 1991; Marotzke and Willebrand, 1991; Mikolajewicz and Maier-Reimer, 1994; Schmittner and Weaver, 2001; Prange *et al.*, 2003; Bryan *et al.*, 2006). These originate from the classic Bryan-Cox model developed in 1960s (Bryan, 1969), and have a long history of application in ocean and climate modeling. Compared to the depth coordinate model, the isopycnic coordinate model is distinctly different in its vertical discretization of the ocean (Chassignet *et al.*, 1996, 2003; Griffies *et al.*, 2000; Bleck, 2002). The depth coordinate model solves the equations using Eulerian methodology in the vertical direction, whereas the isopycnic coordinate model uses Lagrangian (Adcroft and Hallberg, 2006).

Although the development of isopycnic coordinate models lagged depth coordinate models, this class of models and their derivatives (i.e. hybrid or quasi-isopycnic coordinate models) have matured to the point that they are routinely used in both ocean and climate modeling (Chassignet *et al.*, 1996, 2003; Furevik *et al.*, 2003; Hallberg and Gnanadesikan, 2006; Sun and Bleck, 2006; Griffies *et al.*, 2009). Isopycnic coordinate ocean models preserve water masses as they move along isopycnals and therefore more naturally represent the ocean interior. This feature may be particularly advantageous in the simulation of the AMOC (Chassignet *et al.*, 2000; Willebrand *et al.*, 2001). Considering that subgrid-scale parameterization is a function of the vertical coordinate, it is of great interest and importance to

study the performance of the isopycnic coordinate model and its derivatives by comparing their simulations of the AMOC with those from the depth coordinate model.

In the present study, we use the Parallel Ocean Program (POP) ocean model and the HYbrid Coordinate Ocean Model (HYCOM) to simulate the AMOC. POP is a depth coordinate model while HYCOM is primarily an isopycnic coordinate model, with the vertical coordinate smoothly reverting to pressure coordinate in the mixed layer and unstratified oceans (Chassignet *et al.*, 2006). Both models are coupled to the Community Sea Ice Model (CSIM) and forced by repeat Normal Year Forcing (NYF), as described by Large and Yeager (2004) and used in the Coordinated Ocean Research Experiments of Griffies *et al*. (2009). In all cases they are initialized with the same ocean tracer climatologies and a state of rest. By similarly configuring HYCOM and POP, we investigate the impact of the vertical coordinate and salinity boundary conditions on the simulation of the AMOC. The goals are to increase confidence in ocean and climate model solutions and to advance ocean model development. The paper is organized as follows: Section 2 describes the models and forcing. Section 3 presents and compares the simulation results from HYCOM and POP, followed by a discussion and conclusion.

2. Description of Models and Atmospheric Forcing

The depth coordinate POP here is version 2, while the one used by Griffies *et al*. (2009) is version 1 (Smith and Gent, 2004)[1]. The model employs Arakawa B-grid and is configured with the North Pole coordinate singularity displaced over Greenland. The ocean resolutions are 1.125^{o} in the longitudinal direction, while the latitudinal resolution varies from 0.27^{o} at the equator to 0.64^{o} (totally 320x384 grid points). There are 40 vertical levels with the thickness of

[1] POP1.0 and POP2.0 use different advection schemes. Some parameter values for Gent-McWilliams and anisotropic viscosity schemes differ between the two versions. They also employ different salinity restoring strategies under sea ice.

the levels ranging from 10 m at the surface to 250 m in the deep ocean (Table 1). POP uses an isopycnal eddy transport parameterization (Gent and McWilliams, 1990) and an anistropic horizontal viscosity (Large *et al.*, 2001) as generalized by Smith and McWilliams (2003). The *K*-profile parameterization (KPP) of vertical mixing (Large *et al.*, 1994) and an idealized diurnal cycle of solar forcing are also implemented in POP (Danabasoglu *et al.*, 2006). The coefficients of lateral viscosity depend on the local deformation rate (Smagorinsky, 1993). The background vertical diffusivity and viscosity are respectively 0.1 and 1.0 $cm^2\ s^{-1}$. The barotropic equation is solved using an implicit free-surface formulation (Dukowicz and Smith, 1994) and the freshwater flux at the ocean surface is formulated as a virtual salt flux (Yin *et al.*, 2009).

HYCOM (version 2.2) employs Arakawa C-grid and is configured on the same tracer mesh as POP. It has 32 hybrid layers with the layer thickness ranging from 3 dbar (≈3 m) at the surface to several hundred dbar in the ocean interior. Each coordinate surface is assigned a reference isopycnal (Table 2). In the mixed layer or unstratified oceans, vertical grid points are constrained to remain at a fixed depth, but are allowed to join and follow their reference isopycnals over the adjacent deep ocean (Bleck, 2002; Chassignet *et al.*, 2003, 2006). Mesoscale eddy stirring is implemented via layer interface smoothing. Here the model uses the standard nonslab KPP scheme (Halliwell, 2004). The background vertical diffusivity and viscosity are the same as those used by POP. As for POP, HYCOM employs the virtual salt flux method. For overflows, HYCOM has a vertical resolution that naturally migrates to the density front atop a gravity current (Hallberg, 2000). Isopycnic coordinate models have been shown to produce plausible simulations of outflows, including the correct level of entrainment, although such models do show sensitivity to such key parameters as the entrainment rate and the critical

Richardson number (Xu *et al.*, 2007). An improved representation of overflows in HYCOM could have a significant impact on the simulations of the AMOC and the mean climate state.

The prescribed NYF surface forcing includes incident short-wave insolation and downwelling long-wave radiation, surface air temperature and humidity, sea level pressure, wind stress, precipitation and runoff (Large and Yeager, 2004). The heat flux at the ocean surface is determined by

$$F_{heat} = F^*_{rad} + F_{sen}(SST) + F_{lat}(SST) - \sigma(SST)^4 \quad , \tag{1}$$

where σ is the Stefan-Boltzmann constant and F^*_{rad} is the sum of the above prescribed radiative fluxes plus reflected solar, with the asterisk indicating no year-to-year variations. The dependence of the upward long-wave radiation and bulk calculations of both the sensible (F_{sen}) and latent (F_{lat}) heat fluxes on model's prognostic SST gives the flux inter-annual variability.

The surface freshwater water flux (not including restoring flux) is given by

$$\begin{aligned} F_{water} &= F^*_{precip} + F_{evap} + F^*_{runoff} \\ F_{evap}(SST) &= F_{lat} / \lambda \end{aligned} \quad , \tag{2}$$

where λ is the latent heat of vaporization and both precipitation (F^*_{precip}) and runoff (F^*_{runoff}) are prescribed with no inter-annual variability. The heat and water fluxes are partially coupled through the calculation of evaporation (F_{evap}) and latent heat. The freshwater flux is converted to a virtual salt flux with the reference salinity (S_{ref}) set to 35 *psu*:

$$F_{salt} = -F_{water} \cdot S_{ref} \quad . \tag{3}$$

In addition, there can be a salinity restoring term $F_{restore}$ applied at the ocean surface. Although the salinity restoring is unphysical, its use in OGCM maintains a more realistic SSS (Griffies *et al.*, 2009).

The expression for $F_{restore}$ differs between HYCOM and POP. In HYCOM, the restoring salt flux is standard and is calculated according to

$$F_{restore}^{HYCOM} = V_{piston}(SSS_{obs} - SSS_{sim}) \quad , \tag{4}$$

where SSS_{obs} and SSS_{sim} are the observed and simulated values respectively, and V_{piston} is a piston velocity. On the other hand, POP uses anomaly restoring which is expressed as,

$$\begin{aligned} F_{restore}^{POP} &= V_{piston}(SSS'_{obs} - SSS'_{sim}) \\ &= V_{piston}[SSS'_{obs} - SSS_{sim}(x,y,t) + \overline{SSS_{sim}}(t)] \end{aligned} \quad , \tag{5}$$

where SSS'_{obs} and SSS'_{sim} are the deviations from the global means ($\overline{SSS}$) at each time. The anomaly restoring in POP therefore ensures a zero net salt flux associated with $F_{restore}$. The salt flux from anomaly restoring depends on the simulated global mean SSS. It decreases with the decrease in the global mean SSS, making anomaly restoring less effective than standard restoring (shown later). Therefore, standard restoring is designed to prevent the drift of the global mean SSS, while allowing the drift of the global mean salinity. In contrast, anomaly restoring is designed to eliminate the effect of the restoring salt flux on the global mean salinity, while allowing the drift of the global mean SSS. Due to this difference the restoring cases of HYCOM and POP are not directly comparable.

Three cases were integrated with HYCOM and three with POP: no salinity restoring ($V_{piston} = 0$); a weak salinity restoring ($V_{piston} = 50m/4years$); and a strong salinity restoring ($V_{piston} = 50m/300days$). The restoring term is applied globally and uniformly, including under sea ice. The comparison of the two no restoring cases is used to show that the impact of the different vertical coordinate is small, a conclusion already put forward by Griffies *et al.* (2009). The four other restoring integrations reveal a much larger effect of the salinity boundary

condition on the simulation of the AMOC. HYCOM is used to look at the impact of standard restoring and POP to look at the impact of anomaly restoring. Due to the computational expense, all cases were run for only 150 years, which is sufficient to show differences in behavior, but may not be long enough for the equilibration of the AMOC in some models (Griffies *et al.*, 2009). Our conclusions in this paper are based on the 150-year integrations.

3. Results

Figure 1 shows the time evolution of the AMOC as simulated by HYCOM and POP with different salinity restoring. Starting from a resting state, the initial density field almost immediately establishes the AMOC. During the first several years, there is relatively little sensitivity of the AMOC to the salinity boundary condition. After its establishment, however, the AMOC cannot be sustained without a salinity restoring. A difference that may be attributable to the vertical coordinate is the inter-annual variability of the AMOC during model spin-up. With the repeat annual cycle of NYF, such variability can only be generated internally and is only seen in HYCOM. The inter-annual variability of the AMOC is quite pronounced during the first 100 years in the strong restoring case. The initial development of the AMOC variability seems related to the adjustment of the isopycnic surfaces in HYCOM (shown later).

3.1. No Salinity Restoring Case

With no salinity restoring the AMOC rapidly spins down to less than 4 Sv in both HYCOM and POP after 100 years (Fig. 1). The AMOC index is defined as the maximum meridional overturning streamfunction value north of 30°N in the Atlantic Ocean. The meridional streamfunctions (Figs. 2a and 2b) show the shutdown of the clockwise circulation

between about 500 m and 3000 m, although there is a very weak remnant in POP. In HYCOM, a counterclockwise cell associated with the circulation of the Antarctic Intermediate Water (AAIW) develops in the upper 1000 m of the South Atlantic (Fig. 2a), but is confined to the upper 500 m in POP. It has been shown that this cell plays an important role in causing multiple equilibrium states of the AMOC in some climate models (Yin and Stouffer, 2007).

The mixed layer depths in the high-latitude North Atlantic are much too shallow in both cases (Figs. 3b and 3c) in comparison with the observational estimate (Fig. 3a), indicating a complete cessation of the deep convection and deep water formation. In both Figs. 4a and 4b, the meridional velocity in the deep ocean below 1500 m is very sluggish without a pronounced deep western boundary current. The Gulf Stream is a narrow and intense feature, which is associated with strong titling and packing of isopycnals. Its northward mass transport is compensated by the slow, but broad southward flow in the upper ocean.

The collapse of the AMOC results from the continuing decrease of the salinity in the deep convection and deep water formation region of the North Atlantic (Fig. 5b). In both HYCOM and POP, the SSS in the region 60^{o}W-30^{o}E, 50^{o}-80^{o}N decreases from about 34.4 *psu* to a value below 31 *psu* at year 150 - a roughly 3.5 *psu* freshening. This freshening is sufficiently strong to shut down the AMOC in many climate models (Stouffer *et al.*, 2006). In POP the decrease of SSS is faster than in HYCOM during the first 70 years, even though the spin-down of the AMOC is slower (Fig. 1). In terms of the SST in the deep convection region, both models show a decrease from about 5^{o}C to 4^{o}C over 150 years (Fig. 5a). Thus, the decreases in salinity and temperature contribute oppositely to the fractional change in the surface density given by:

$$\delta\rho / \rho_0 = \beta\delta S - \alpha\delta T \quad . \tag{6}$$

But with $\alpha = 1.7 \times 10^{-4}$ $^{o}C^{-1}$, $\beta = 7.6 \times 10^{-4}$ at these latitudes, the freshening dominates the cooling by an order of magnitude on the right hand side of Eq. 6, leading to lighter surface water. The negative feedback between SST and surface heat flux is evident. With the ocean cooling in the deep convection region, the heat loss from the ocean to the atmosphere reduces by roughly 40 W/m^2 (Fig. 5c), counteracting the decrease in SST. In contrast, there is no such feedback between SSS and freshwater flux, so in both models the freshwater flux into the ocean continually increases after establishment of the AMOC (Fig. 5d) in response to the reduced evaporation due to the cooler SSTs (Eqs. 1 and 2), while precipitation remains as prescribed. The geographical distribution of the freshwater flux is quite similar between HYCOM and POP (Figs. 6a and 6b).

With no salinity restoring, the geographical distribution of the SST biases compared to the observation shows that there is a regional and moderate 3^{o}C cooling in the high-latitude North Atlantic in both HYCOM and POP (Figs. 7b and 7c), resulting from the shutdown of the AMOC and the reduction of the northward heat transport in the Atlantic. But the spread of the cooling to other ocean regions is not evident due to the constraint of the prescribed atmosphere. In contrast, fully coupled AOGCMs showed that a shutdown of the AMOC can lead to a 10^{o}-15^{o}C ocean surface cooling in the northern North Atlantic, and that the cooling can spread over the entire North Atlantic (Yin and Stouffer, 2007). Both HYCOM and POP show problems common in contemporary coarse resolution ocean climate models, such as the displacement of the Gulf Stream and the warm biases along the coastal region (Large and Danabasoglu, 2006). However, HYCOM exhibits larger warm biases than in POP in the Southern Ocean.

In terms of SSS, a significant freshening occurs in the high-latitude North Atlantic in both models (Figs. 8b and 8c). This large freshening illustrates that SSS can evolve more freely

than SST due to the mixed boundary conditions (Mikolajewicz and Maier-Reimer, 1994). After a freshwater cap forms in the northern North Atlantic, it propagates southward with the gyre circulation into the tropical and South Atlantic. The pattern is very similar to the results from the so-called "water-hosing" experiment (Yin and Stouffer, 2007), although no external freshwater addition is imposed in the present study.

The most significant difference between the formulations of HYCOM and POP is the vertical coordinate. So it is of interest to compare the vertical distribution of temperature, salinity and therefore water masses as modeled by HYCOM and POP. In HYCOM, the vertical coordinate is isopycnic in the ocean interior, but smoothly reverts to pressure coordinate in the upper and polar oceans, where the ocean stratification is weak and deep convection takes place (Figs. 9 and 10). It should be noted that due to the shutdown of the AMOC and the surface freshening in the high-latitude North Atlantic, the vertical coordinate in the upper ocean north of 40^{o}N is isopycnic in HYCOM (Figs. 9b and 10b). In low and middle latitudes, isotherms are almost parallel to the isopycnic interfaces, as temperature dominates salinity in determining the seawater density there. The upper warm water penetrates more deeply in POP (Fig. 9c).

In terms of salinity, the freshening occurs only in the surface layer in POP, so that the salinity below 300 m is high when compared to that in HYCOM (Figs. 10b and 10c). In contrast, the freshening penetrates more deeply in HYCOM, so the salinity in the entire North Atlantic is lower (Fig. 10b). In the South Atlantic, the northward intrusion of AAIW is distinguishable in both HYCOM and POP, as shown by the fresh tongue in 500-1000 m depth. AAIW reaches further north in HYCOM, so that it connects to the freshening region in the North Atlantic. However, the northward intrusion of AAIW is relatively weak in almost all model runs when compared to the observation (Fig. 10a).

3.2. Salinity Restoring Cases

The AMOC and related fields are much more sensitive to the salinity boundary condition than to the vertical coordinate's choice. In all restoring cases, the upwelling of NADW mainly occurs outside of the Atlantic basin and the AMOC is the dominant feature in the Atlantic (Fig. 2). However, coordinate differences may contribute to the large Southern Ocean changes in ocean temperature (Figs. 7 and 9) and salinity (Fig. 10), seen in HYCOM relative to POP. Otherwise, salinity restoring can be described as systematically increasing the strength of the AMOC at 150 years, with weak anomaly, weak standard, strong anomaly and strong standard restoring producing progressively stronger AMOC (Fig. 2). This pattern of response is also indicated by the inter-basin exchange across 30^{o}S and the high-latitude salinities (Fig. 10).

Some responses are characterized by another pattern, from weak anomaly to strong anomaly to weak standard and finally to strong standard restoring. Notable examples of this pattern are deep convection implied by mixed layer depths (Fig. 3), the deep western boundary current (Fig. 4), the SSS at years 141-150 (Fig. 5), and the SST cold bias (Fig. 7). The overflow across the Greenland-Iceland-Scotland ridge displays a more complicated pattern. It is evident only in the four restoring cases of Fig. 10 and characterized by the fresh tongue around 50^{o}N and between 1500 to 3000 m. Further results are now discussed separately for HYCOM and POP, since they use different formulas for salinity restoring (Eqs. 4 and 5, respectively).

3.2.1. Standard Restoring in HYCOM

The AMOC can be sustained in HYCOM once a weak salinity restoring ($V_{piston} = 50m/4years$) is applied at the ocean surface. The AMOC first spins down with a slower rate of decrease than in the no restoring case. It eventually stabilizes at about 12 Sv after

100 years (Fig. 1). It should be noted that the definition of the AMOC index here differs from the one used by Griffies *et al.* (2009). Therefore, Fig. 1 here cannot be compared directly to Fig. 25 in Griffies *et al.* (2009). Due to the relatively weak AMOC, the intra- and inter-basin exchanges of seawater are also weak. There is approximately 4 Sv inter-hemispheric exchange of seawater and 8 Sv of exchange at 30^{o}S associated with the AMOC (Fig. 2c). The AMOC remains active because the fresh salinity biases seen in Fig. 8b are much reduced by the salinity restoring (Fig. 8d). The SSS in the deep convection region decreases only by 0.1 *psu* during the 150-year integration, in contrast to more than 3 *psu* in the no restoring case (Fig. 5b). Thus the salinity restoring is effective at modifying the total water flux in the deep convection region (Figs. 5d and 6c) and therefore controlling salinity drift in HYCOM. As a result of the active AMOC, a deep western boundary current is simulated just beneath the Gulf Stream at about 2500 m depth (Fig. 4c). Meanwhile, the Gulf Stream accelerates, transporting more water mass northward to compensate both the upper southward gyre circulation and the deep western boundary current.

The deep convection in the North Atlantic is realistic and takes place in 4 regions: near the south tip of Greenland; the Irminger Sea; south of Iceland; and the Nordic Seas (Figs. 3a and 3d). Due to the deep convection, upper ocean stratification is weak in the high-latitude North Atlantic and the vertical coordinate in HYCOM transitions from isopycnals to pressure coordinate (Figs. 9d and 10d). The mode water in the subtropical North Atlantic, which is characterized by salinity greater than 35 *psu*, can penetrate to a greater depth (Fig. 10d). Generally, the spread of different water masses along different isopycnals is more pronounced in HYCOM than in POP.

The AMOC is most vigorous and realistic in the strong salinity restoring case ($V_{piston} = 50m/300days$). The mean strength of the AMOC during the last 20 years of the integration is about 17 Sv (Fig. 1), consistent with observational estimates (Ganachaud, 2003; Talley, 2003). The intra- and inter-basin exchanges of seawater are strong, leading to large heat and freshwater redistribution in the ocean. Consistent with a strong AMOC, the speed of the deep western boundary current can exceed 3 cm/s at 30^{o}N (Fig. 4e). A large part of the convection in the Labrador Sea and Nordic Seas is open ocean convection (Fig. 3f). While the strong restoring keeps the simulated SSS very close to the observed (Fig. 8f), the SST biases persist (Figs. 7b, 7d and 7f), implying that they are not caused by the salinity drift.

The AMOC in HYCOM shows some variability during the spin-up period, which becomes weaker after 100 years (Fig. 1). Some fully coupled AOGCMs show much stronger variability of the AMOC (Stouffer *et al.*, 2006). The mechanism that causes variations of the AMOC in the uncoupled OGCM differs from that in the fully coupled AOGCM. The variability of the AMOC in many AOGCMs is the ocean response to the noisy atmospheric fluxes (Delworth *et al.*, 1993; Griffies and Tziperman, 1995; Greatbatch and Delworth, 2000). Because the atmosphere is prescribed in the present study, the variability of the AMOC in HYCOM is an ocean-only mode which is induced by ocean internal processes. It is likely related to the initial adjustment of isopycnic surfaces. The thickness of the North Atlantic Deep Water layers ($36.38<\sigma_2<36.97$, layers 18-25) at 30^{o}N of the Atlantic undergoes large variability during the first 100 years (Fig. 11). This adjustment of isopycnic surfaces also occurs in other studies with HYCOM (Sun and Bleck, 2006; Chassignet *et al.*, 2006). The layer thickness directly influences the meridional mass transport in the deep ocean, contributing to the variability of the AMOC. In addition, the mechanism may be linked to wave sloshing and needs to be further investigated.

3.2.2. Anomaly Restoring in POP

The AMOC is active, but weak (6 Sv) in the weak salinity restoring case (Fig. 1). Figure 2d shows that this restoring adds about 2 Sv of overturning north of 60^{o}N, which gives most of the increase in the streamfunction above 2500 m in the South Atlantic. This picture is consistent with NADW formation only at the northern Nordic Seas, without any deep convection and deep water formation in the Labrador Sea and the region south of the Greenland-Scotland ridge (Fig. 3e). The POP results presented in this paper are not directly comparable to those presented in Griffies *et al.* (2009) because *a*) of the use of POP version 2 instead of version 1 and *b*) POP in Griffies *et al.* (2009) employs different salinity restoring under sea ice. Weak anomaly restoring is not very effective at modifying the water flux in the deep convection region (Figs. 5d and 6d) and at preventing a salinity drift (Figs. 5b and 8e). The main reason is that the global mean SSS decreases by about 0.3 *psu* (Fig. 12) and the resulting restoring salt flux inhibits the deep convection in the Labrador Sea and south of the Greenland-Scotland ridge (Eq. 5 and Fig. 3e). The SSS in the deep convection region decreases by about 1 *psu* during the first 70 years before the salinity restoring tends to prevent any further decrease (Fig. 5b). Geographically, there is still a pronounced freshening north of 40^{o}N by the end of the integration (Figs. 8e and 10e). The cooling of about 0.5^{o}C partially counteracts the freshening and stabilizes the surface water density (Fig. 5a). Compared to that in the no restoring case, the reduction of the heat loss is smaller due to the smaller cooling (Fig. 5c).

With strong anomaly restoring, the AMOC spins down very slowly and reaches about 14 Sv by the end of the integration (Fig. 1). This stronger AMOC results from the more realistic SSS in the deep water formation region (Figs. 5b and 8g). This state is achieved while not allowing restoring to change the global ocean salt content. Since the global mean SSS decreases

by about 0.2 *psu* (Fig. 12), this makes the strong anomaly restoring less effective than the strong standard restoring at modifying the freshwater flux (Fig. 6). The slow weakening of the AMOC during the first 100 years is also a result of a warming in the deep convection region (Fig. 5a). The heat loss to the atmosphere increases during the first 10 years and then gradually returns to the initial value (Fig. 5c), leading to a stabilization of the AMOC.

Vigorous deep convection and deep water formation takes place in the Labrador Sea and Nordic Seas, and in the region south of the Greenland-Scotland ridge (Fig. 3g). Notice that the deep convection sites in the Labrador Sea and Nordic Seas are close to the sea ice margin where sea ice melting takes place. The deep convection is mainly controlled by intense winter heat loss. In the strong restoring case, the ocean interior of the northern North Atlantic is warmer and more saline due to the strong northward transport of heat and salt by the AMOC (Figs. 9 and 10).

4. Discussion and Conclusion

The present study uses two distinctly different ocean models to simulate the Atlantic meridional overturning circulation. One model is the depth coordinate POP; the other is the quasi-isopycnic coordinate HYCOM. By comparing the simulation of the AMOC and closely related fields, the present study is the first step to achieve our ultimate goal, that is, to systematically investigate the impact of the vertical coordinate and salinity boundary condition on ocean climate simulations. In general, the performances of the two models are qualitatively similar in terms of the AMOC modeling. By running similarly configured HYCOM and POP coupled to the same sea-ice model with identical prescribed atmospheric forcing, it is found that neither HYCOM nor POP can maintain an active AMOC without the application of salinity restoring. The two no salinity restoring cases are the only two directly comparable cases in this

study. It shows that the two models behave in a similar fashion, with all the differences between them being smaller than the differences induced by salinity restoring (Figs. 2-10).

With no salinity restoring, the shutdown of the AMOC appears to be a consequence of it being established with too little northward transport of heat and salt into the high latitude source regions of the North Atlantic to balance the 50 to 60 W/m^2 of surface heat loss and the 2 to 3 mm/day of freshwater input. As the SST and SSS decrease in response, there is less net heat loss and hence a negative feedback to the SST decrease, but the reduced evaporation continues to add to the freshening. The salinity decrease and domination of salinity over temperature in determining the water density combine to produce lighter surface water, which leads to a weaker AMOC and even less northward transport of heat and freshwater. This positive feedback continues to weaken the AMOC until it collapses. After 150 years, the approximate 1^oC decrease in SST reduces the heat loss by 30 to 40 W/m^2. The approximate 3 *psu* lower salinity means that the density is lighter by more than 2 kg/m^3. SSS and surface density will presumably continue to decrease until the gyre circulation is able to transport sufficient salt to maintain the fresher and lighter surface water.

Salinity restoring is a simple, but artificial means of overcoming the above positive feedback by introducing a negative feedback into the system. The AMOC remains active once salinity restoring is applied, and is strong in the strong restoring cases. Strong restoring is most effective when applied in the standard fashion than applied as anomaly. The reason is that the anomaly restoring flux depends on the simulated global mean SSS, which decreases in all cases of the POP simulation. Griffies *et al*. (2009) discussed other methods of salinity restoring and present the sensitivity of other models. They showed that the standard POP salinity boundary

condition of weak anomaly restoring of SSS together with a precipitation adjustment produces an acceptable AMOC (13 Sv) in an earlier version of POP (version 1) driven by CORE NYF.

Due to the sharply different vertical discretization between HYCOM and POP, the similarities between HYCOM and POP indicate robust results. The results confirm that the thermohaline forcing, especially the salinity boundary condition and freshwater forcing at the ocean surface, plays a distinctive and crucial role in simulating the AMOC. Except for the salinity boundary condition, all other forcings, including wind stress and model parameters such as for diapycnal mixing, are the same between different cases. The simulated anemic, weak and strong AMOCs in the three cases suggest that proper thermohaline fluxes are among the most important and difficult issues in the AMOC modeling, especially when the ocean model is coupled to the atmospheric model and when salinity restoring should not be used.

With repeat NYF, the AMOC collapses in the uncoupled ocean model unless there is some unphysical freshwater flux. However, the AMOC is typically strong when ocean models such as POP are coupled to the atmospheric models, even though the atmospheric fluxes in the coupled system may deviate greatly from observational estimates and there is no salinity restoring. One possible explanation is that the maintenance of the AMOC may depend critically on extremely cold winters, which are missing in repeat NYF. A better understanding of the reason for AMOC maintenance in AOGCMs would be very useful for model development and ocean climate simulation, where an important goal must be generate a stable and vigorous AMOC without any unphysical salinity restoring. Until then it is difficult to go beyond the present study where the simulations of the components of the AMOC, including ocean currents, overflow, and water mass distribution are either far from nature, or confused by unphysical boundary conditions.

Acknowledgements

This research is supported by the Office of Science of US Department of Energy (grant #DE-FG02-07ER64470). We wish to thank G. Caldwell, S. Dean, M. Field, S. Griffies, G. Peng, J. Rew and two anonymous reviewers for comments and helps. The computation was supported by the Climate Simulation Laboratory of National Center for Atmospheric Research and the Breakthrough Science Computation of National Science Foundation.

References

Adcroft, A., Hallberg, R., 2006. On methods for solving the oceanic equations of motion in generalized vertical coordinates. Ocean Modell. 11, 224-233.

Bleck, R., 2002. An oceanic general circulation model framed in hybrid isopycnic-Cartesian coordinates. Ocean Modell. 4, 55-88.

Bryan, F., 1986. High-latitude salinity effects and interhemispheric thermohaline circulations. Nature 323, 301-304.

Bryan, F. O., Danabasoglu, G., Nakshiki, N., Yoshida, Y., Kim, D. -H., Tsutsui, J., Doney, S. C., 2006. Response of the North Atlantic thermohaline circulation and ventilation to increasing CO_2 in CCSM3. J. Clim. 19, 2382-2397.

Bryan, K., 1969. Climate and the ocean circulation III: The ocean model. Mon. Wea. Rev. 97, 806-827.

Chassignet, E. P., Smith, L. T., Bleck, R., Bryan, F. O., 1996. A Model Comparison: Numerical Simulations of the North and Equatorial Atlantic Ocean Circulation in Depth and Isopycnic Coordinates. J. Phys. Oceanogr. 26, 1849-1867.

Chassignet, E. P., Arango, H., Dietrich, D., Ezer, T., Ghil, M., Haidvogel, D. B., Ma, C.-C., Mehra, A., Paiva, A. M., Sirkes, Z., 2000. DAMÉE-NAB: The base experiments. Dyn. Atmos. Oceans 32, 155-184.

Chassignet, E. P., Smith, L. T., Halliwell, G. R., Bleck, R., 2003. North Atlantic simulation with the HYbrid Coordinate Ocean Model (HYCOM): Impact of the vertical coordinate choice, reference density, and thermobaricity. J. Phys. Oceanogr. 33, 2504-2526.

Chassignet, E. P., Hurlburt, H. E., Smedstad, O. M., Halliwell, G. R., Wallcraft, A. J., Metzger, E. J., Blanton, B. O., Lozano, C., Rao, D. B., Hogan, P. J., Srinivasan, A., 2006.

Generalized vertical coordinates for eddy-resolving global and coastal ocean forecasts. Oceanography 19, 20-31.

Danabasoglu, G., Large, W. G., Tribbia, J. J., Gent, P. R., Briegleb, B. P., 2006. Diurnal Coupling in the Tropical Oceans of CCSM3. J. Clim. 19, 2347-2365.

Delworth, T. L., Manabe, S., Stouffer, R. J., 1993. Interdecadal variations of the thermohaline circulation in a coupled ocean-atmosphere model. J. Clim. 6(11), 1993-2011.

Delworth, T. L., Greatbatch, R. J., 2000. Multidecadal thermohaline circulation variability driven by atmospheric surface flux forcing. J. Clim., 13(9), 1481-1495.

de Boyer Montégut, C., Madec, G., Fischer, A. S., Lazar, A., Iudicone, D., 2004. Mixed layer depth over the global ocean: an examination of profile data and a profile-based climatology, J. Geophys. Res. 109, C12003, doi:10.1029/2004JC002378.

Dukowicz, J. K., Smith, R. D., 1994. Implicit free-surface method for the Bryan-Cox-Semtner ocean model, J. Geophys. Res. 99(C4), 7991–8014.

Furevik, T., et al., 2003. Description and evaluation of the Bergen climate model: ARPEGE coupled with MICOM. Clim. Dyn. 21, 27–51.

Ganachaud, A., 2003. Large-scale mass transports, water mass formation, and diffusivities estimated from World Ocean Circulation Experiment (WOCE) hydrographic data. J. Geophys. Res. 108, 3213.

Gent, P. R., McWilliams, J. C., 1990. Isopycnal mixing in oceancirculation models, J. Phys. Oceanogr. 20, 150–155.

Griffies, S. M., Tziperman, E., 1995. A linear thermohaline oscillator driven by stochastic atmospheric forcing. J. Clim., 8(10), 2440-2453.

Griffies, S. M., Boning, C., Bryan, F. O., Chassignet, E. P., Gerdes, R., Hasumi, H., Hirst, A., Treguier, A.-M., Webb, D., 2000. Developments in Ocean Climate Modelling. Ocean Modell. 2, 123-192.

Griffies, S. M., Biastoch, A., Boning, C., Bryan, F., Chassignet, E., Danabasoglu, G., England, M. H., Gerdes, R., Haak, H., Hallberg, R. W., Hazeleger, W., Jungclaus, J., Large, W. G., Madec, G., Samuels, B. L., Scheinert, M., Severijns, C. A., Simmons, H. L., Treguier, A. M., Winton, M., Yeager, S., Yin, J., 2009. Coordinated Ocean-ice Reference Experiments (COREs). Ocean Modell. 26, 1-46.

Hallberg, R., 2000. Time integration of diapycnal diffusion and Richardson number-dependent mixing in isopycnal coordinate ocean models. Mon. Wea. Rev. 128, 1402-1419.

Hallberg, R., Gnanadesikan, A., 2006. The role of eddies in determining the structure and response of the wind-driven Southern Hemisphere overturning: Results from the Modeling Eddies in the Southern Ocean (MESO) project. J. Phys. Oceanogr. 36, 2232-2251.

Halliwell, G. R., 2004. Evaluation of vertical coordinate and vertical mixing algorithms in the hybrid-coordinate ocean model (HYCOM). Ocean Modell. 7, 285-322.

Large, W. G., McWilliams, J. C., Doney, S. C., 1994. Ocean verticalmixing: A review and a model with a nonlocal boundary layer parame-terization, Rev. Geophys. 32, 363–403.

Large W. G., Danabasoglu, G., McWilliams, J. C., Gent, P. R., Bryan, F. O., 2001. Equatorial circulation of a global ocean climate model with aniostropic horizontal viscosity. J. Phys. Oceanogr. 31, 518-536.

Large, W. G., Yeager, S., 2004. Diurnal to decadal global forcing for ocean and sea-ice models: the data sets and flux climatologies. NCAR Technical Note: NCAR/TN-460+STR. CGD Division of the National Center for Atmospheric Research.

Large, W. G., Danabasoglu, G., 2006. Attribution and impacts of upper ocean biases in CCSM3. J. Clim. 19, 2325-2346.

Manabe, S., Stouffer, R. J., 1988. Two Stable Equilibria of a Coupled Ocean-Atmosphere Model. J. Clim. 1, 841-866.

Marotzke, J., Willebrand, J., 1991. Multiple equilibria of the global thermohaline circulation. J. Phys. Oceanogr. 21, 1372-1385.

Meehl, G. A., Stocker, T. F., Collins, W. D., Friedlingstein, P., Gaye, A. T., Gregory, J. M., Kitoh, A., Knutti, R., Murphy, J. M., Noda, A., Raper, S. C. B., Watterson, I. G., Weaver, A. J., Zhao, Z.-C., 2007. Global Climate Projections. In: Climate Change 2007: The Physical Science Basis. Contribution of Working Group I to the Fourth Assessment Report of the Intergovernmental Panel on Climate Change [Solomon, S., D. Qin, M. Manning, Z. Chen, M. Marquis, K.B. Averyt, M. Tignor and H.L. Miller (eds.)]. Cambridge University Press, Cambridge, United Kingdom and New York, NY, USA.

Mikolajewicz, U., Maier-Reimer, E., 1994. Mixed boundary conditions in ocean general circulation models and their influence on the stability of the model's conveyor belt, J. Geophys. Res. 99, 22,633–22,644.

Paiva, A. M., Chassignet, E. P., 2001. The impact of surface flux parameterizations on the modeling of the North Atlantic Ocean. J. Phys. Oceanogr. 31, 1860-1879.

Prange, M., Lohmann, G., Paul, A., 2003. Influence of vertical mixing on the thermohaline hysteresis: analyses of an OGCM. J. Phys. Oceanogr. 33, 1707-1721.

Rahmstorf, S., 1995. Bifurcations of the Atlantic thermohaline circulation in response to changes in the hydrological cycle. Nature 378, 145-149.

Schiller, A., Mikolajewicz, U., Voss, R., 1997. The stability of the thermohaline circulation in a coupled ocean–atmosphere model. Climate Dyn. 13, 325–348.

Schmittner, A., Weaver, A. J., 2001. Dependence of multiple climate states on ocean mixing parameters. Geophys. Res. Lett. 28, 1027-1030.

Schmittner, A., Latif, M., Schneider, B., 2005. Model Projections of the North Atlantic thermohaline circulation for the 21st century assessed by observations, Geophys. Res. Lett. 32, L23710, doi:10.1029/2005GL024368.

Smagorinsky J., 1993. Some historical remarks on the use of nonlinear viscosities. Large Eddy Simulation of Complex Engineering and Geophysical Flows, B. Galperin and S. A. Orszag, Eds. Cambridge University Press, pp3–36.

Smith, R. D., McWilliams, J. C., 2003. Anisotropic horizontal viscosity for ocean models. Ocean Modell. 5, 129-156.

Smith, R., Gent, P., 2004. Reference manual for the Parallel OceanProgram (POP) ocean component of the Community Climate SystemModel (CCSM2.0 and 3.0), LAUR-02-2484, Los Alamos Natl. Lab. Los Alamos, N. M.

Steele, M., Morfley, R., Ermold, W., 2001. PHC: A global ocean hydrography with a high-quality Arctic Ocean, J. Clim. 14, 2079-2087.

Stocker, T. F, Wright, D. G., 1991: Rapid transitions of the ocean's deep circulation induced by changes in the surface water fluxes, Nature 351, 729-732.

Stommel, H. M., 1961. Thermohaline convection with two stable regimes of flow, Tellus 13, 224-230.

Stouffer, R. J., Yin, J., Gregory, J. M., Dixon, K. W., Spelman, M. J., Hurlin, W., Weaver, A. J., Eby, M., Flato, G. M., Hasumi, H., Hu, A., Jungclaus, J. H., Kamenkovich, I. V., Levermann, A., Montoya, M., Murakami, S., Nawrath, S., Oka, A., Peltier, W. R., Robitaille, D. Y., Sokolov, A., Vettoretti, G., Weber, S. L., 2006. Investigating the causes of the response of the thermohaline circulation to past and future climate changes. J. Clim. 19, 1365-1387.

Sun, S., Bleck, R., 2006. Multi-century simulations with the coupled GISS-HYCOM climate model: Control experiments, Clim. Dynam. 26, 407-42.

Talley, L. D., 2003. Shallow, intermediate, and deep overturning components of the global heat budget. J. Phys. Oceanogr. 33, 530–560.

Vellinga, M., Wood, R., 2002. Global climatic impacts of a collapse of the Atlantic thermohaline circulation, Clim. Change 54, 251– 267.

Willebrand, J., et al., 2001. Circulation characteristics in three eddy-permitting models of the North Atlantic, Prog. Oceanogr. 48, 123–161.

Xu, X., Chang, Y. S., Peters, H., Özgökmen, T. M., Chassignet, E. P., 2006. Parameterization of gravity current entrainment for ocean circulation models using a high-order 3D nonhydrostatic spectral element model. Ocean Modell. 14, 19-44.

Yin, J., Stouffer, R. J., 2007. Comparison of the Stability of the Atlantic Thermohaline Circulation in Two Coupled Atmosphere-Ocean General Circulation Models. J. Clim. 20, 4293-4315.

Yin, J., Stouffer, R. J., Spelman, M. J., Griffies, S. M., 2009. Evaluating the uncertainty induced by the virtual salt flux assumption in climate simulations and future projections. J. Clim. (in press).

Table 1. The depth of model layers in POP (m).

Layer	Depth	Layer	Depth	Layer	Depth	Layer	Depth
1	5	11	130	21	729	31	3125
2	15	12	149	22	918	32	3375
3	25	13	171	23	1139	33	3625
4	36	14	198	24	1379	34	3875
5	47	15	229	25	1626	35	4125
6	58	16	268	26	1875	36	4375
7	70	17	318	27	2125	37	4625
8	83	18	381	28	2375	38	4875
9	97	19	466	29	2625	39	5125
10	112	20	579	30	2875	40	5375

Table 2. The prescribed target densities for layers in HYCOM.

Layer	σ_2	Layer	σ_2	Layer	σ_2	Layer	σ_2
1	28.10	9	33.15	17	36.20	25	36.97
2	28.90	10	33.70	18	36.38	26	37.02
3	29.70	11	34.25	19	36.52	27	37.06
4	30.50	12	34.75	20	36.62	28	37.10
5	30.95	13	35.15	21	36.70	29	37.17
6	31.50	14	35.50	22	36.77	30	37.30
7	32.05	15	35.80	23	36.83	31	37.42
8	32.60	16	36.04	24	36.89	32	37.48

Figure Legends

Figure 1. Time evolution of the AMOC in the runs without salinity restoring ("NO") and with weak ("WEAK") and strong ("STRONG") salinity restoring. The AMOC index is defined as the maximum meridional overturning streamfunction value north of 30^{o}N in the Atlantic.

Figure 2. The AMOC streamfunction patterns (Sv) simulated by HYCOM and POP with different salinity boundary conditions (mean of the last 10 years). Positive values indicate clockwise circulation. (a), (c) and (e): HYCOM; (b), (d) and (f): POP; (a) and (b): no salinity restoring case; (c) and (d): weak salinity restoring case; (e) and (f): strong salinity restoring case.

Figure 3. Annual mean mixed layer depth (m) in the deep convection region of the AMOC. (a) The observational estimate; (b), (d) and (f): HYCOM; (c), (e) and (g): POP; (b) and (c): no salinity restoring case; (d) and (e): weak salinity restoring case; (f) and (g): strong salinity restoring case. The observational estimate of mixed layer depth is derived from monthly mean climatology of potential temperature and salinity (Griffies *et al.*, 2009).

Figure 4. The meridional velocity (cm/s) at 30^{o}N of the Atlantic (mean of the last 10 years). The data are plotted on the native grids of HYCOM and POP. The interfaces of the hybrid layers in HYCOM are indicated by the black curves. The numbers show the interface index.

Figure 5. Time evolution of the SST, SSS, heat and water fluxes averaged in the deep convection and deep water formation region of the AMOC (50^{o}-80^{o}N, 60^{o}W-30^{o}E). Positive

fluxes indicate a transport from the atmosphere to the ocean. (a) SST (^{o}C); (b) SSS (*psu*); (c) heat flux (W/m^2); (d) water flux (mm/day).

Figure 6. Geographical distribution of the total freshwater flux (mm/day) including the restoring part in HYCOM and POP.

Figure 7. Geographical distribution of the SST biases (^{o}C). (a) The SST observation (Steele *et al.*, 2001); (b), (d) and (f): biases in HYCOM; (c), (e) and (g): biases in POP; (b) and (c): no salinity restoring case; (d) and (e): weak salinity restoring case; (f) and (g): strong salinity restoring case. The values show the simulation (mean of the last 10 years) minus the observation.

Figure 8. Same as Fig. 7, but for the SSS biases (*psu*). Notice that (d) and (e) use different scales.

Figure 9. The latitude-depth cross-section of ocean temperature (^{o}C) along 30^{o}W in the Atlantic. The data (shading) are plotted on the native grid of HYCOM and POP. Green lines show the temperature biases (interval=2.0) and black ones show sample isopycnals.

Figure 10. Same as Fig. 9, but for salinity (*psu*). Green lines show the salinity biases (interval=0.5).

Figure 11. Changes in layer thickness (m) at 30^{o}N of the Atlantic in HYCOM. The values indicate the deviation from the long-term mean. Red curves show the layers that are occupied by North Atlantic Deep Water.

Figure 12. Time series of the global mean SSS (*psu*) in HYCOM and POP.

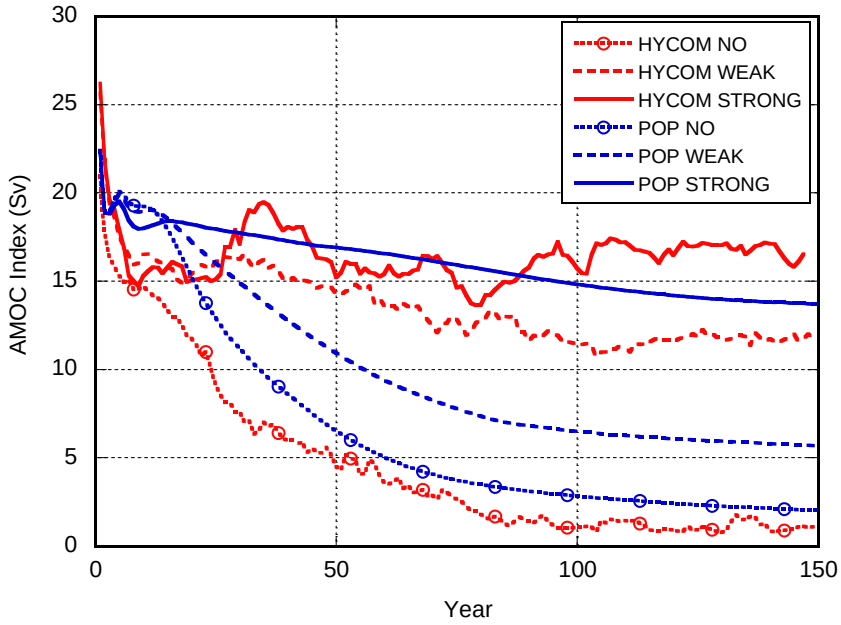
30
25
20
15
10
5
0
0
50
100
150
AMOC Index (Sv)
Year
HYCOM NO
HYCOM WEAK
HYCOM STRONG
POP NO
POP WEAK
POP STRONG

Figure 1

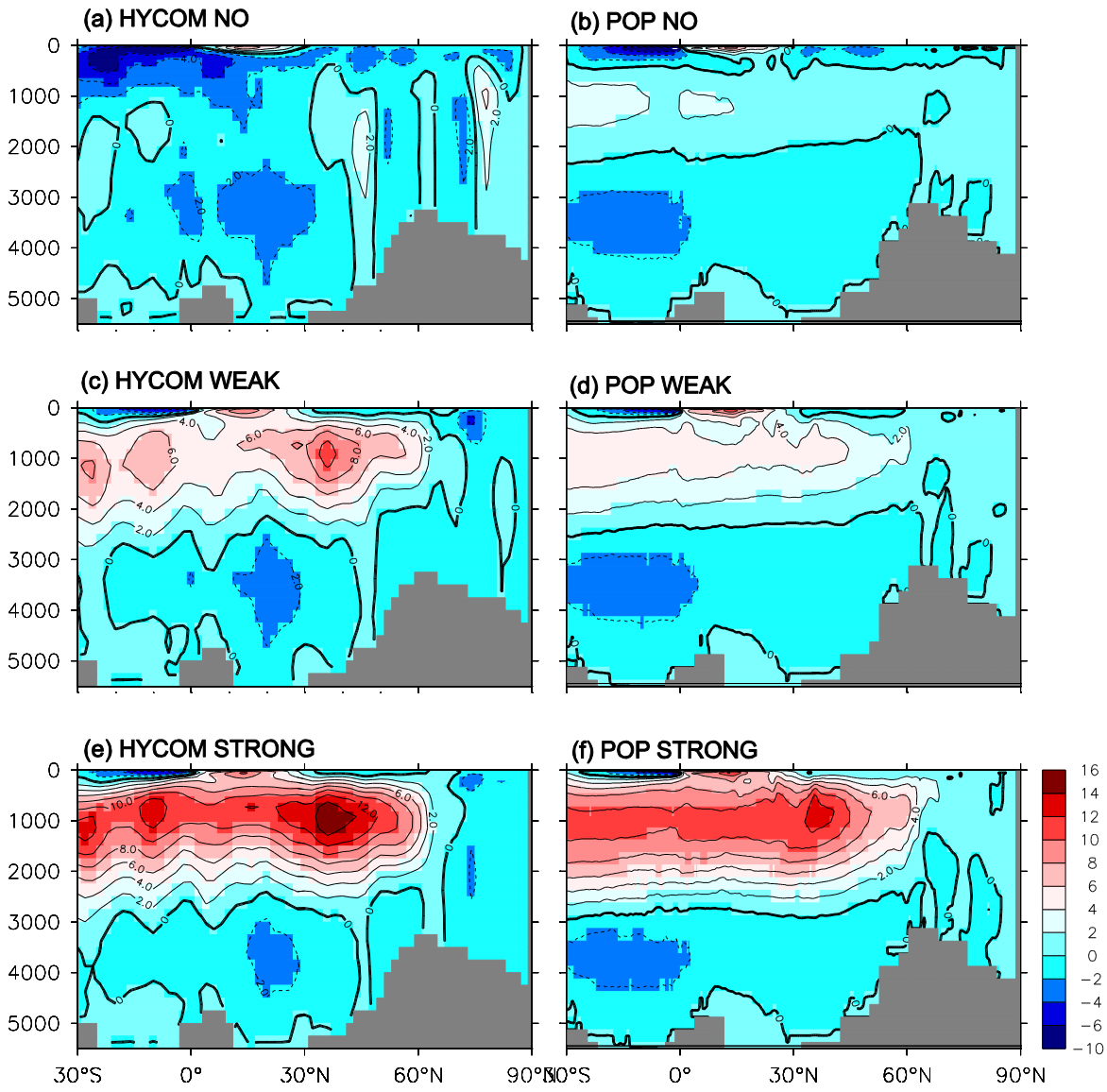
(a) HYCOM NO
(b) POP NO
(c) HYCOM WEAK
(d) POP WEAK
(e) HYCOM STRONG
(f) POP STRONG
0
1000
2000
3000
4000
5000
30°S
0°
30°N
60°N
90°N
16
14
12
10
8
6
4
2
0
−2
−4
−6
−10

Figure 2

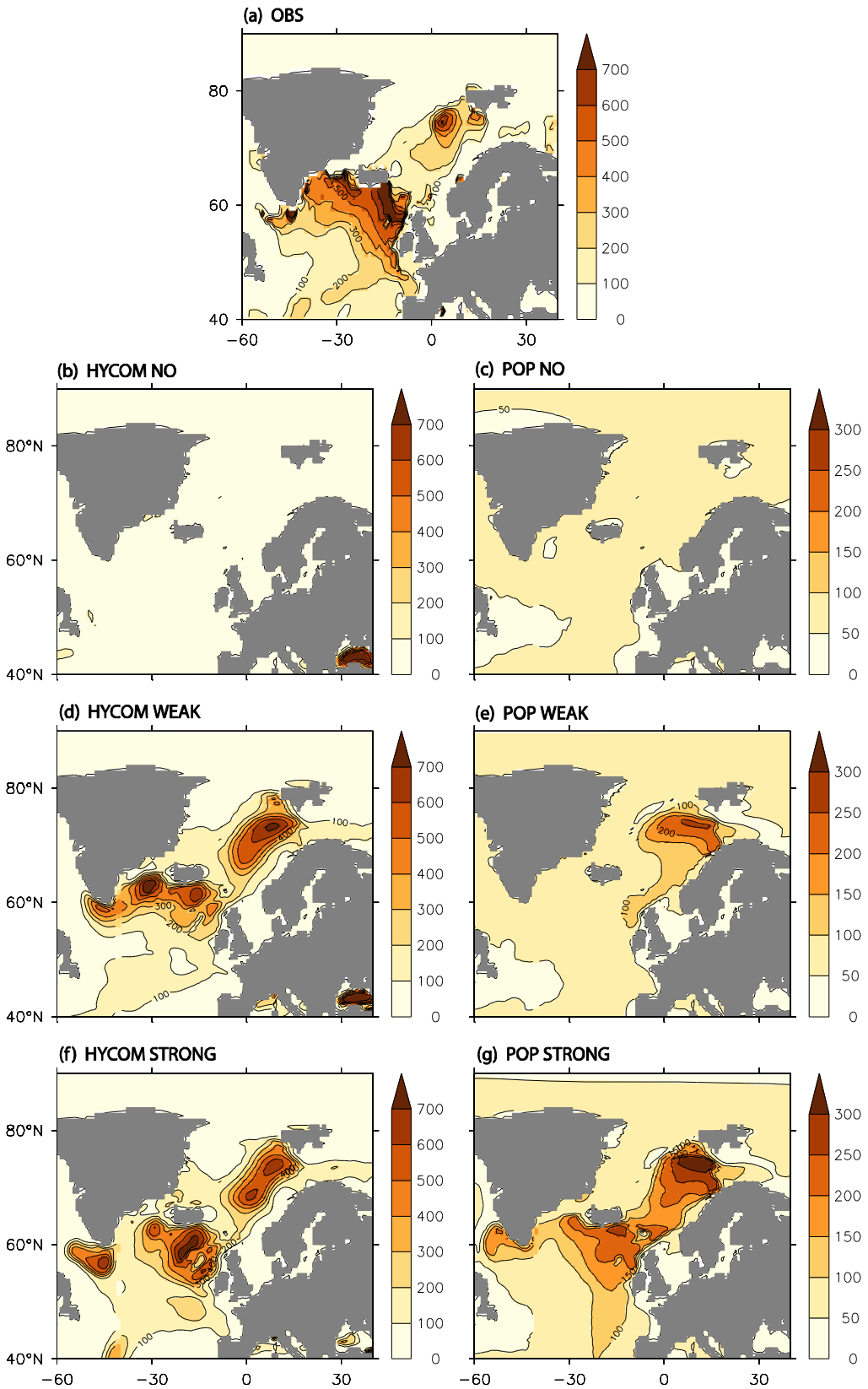
(a) OBS
(b) HYCOM NO
(c) POP NO
(d) HYCOM WEAK
(e) POP WEAK
(f) HYCOM STRONG
(g) POP STRONG
80
60
40
80°N
60°N
40°N
−60
−30
0
30
700
600
500
400
300
200
100
0
300
250
200
150
100
50
0

Figure 3

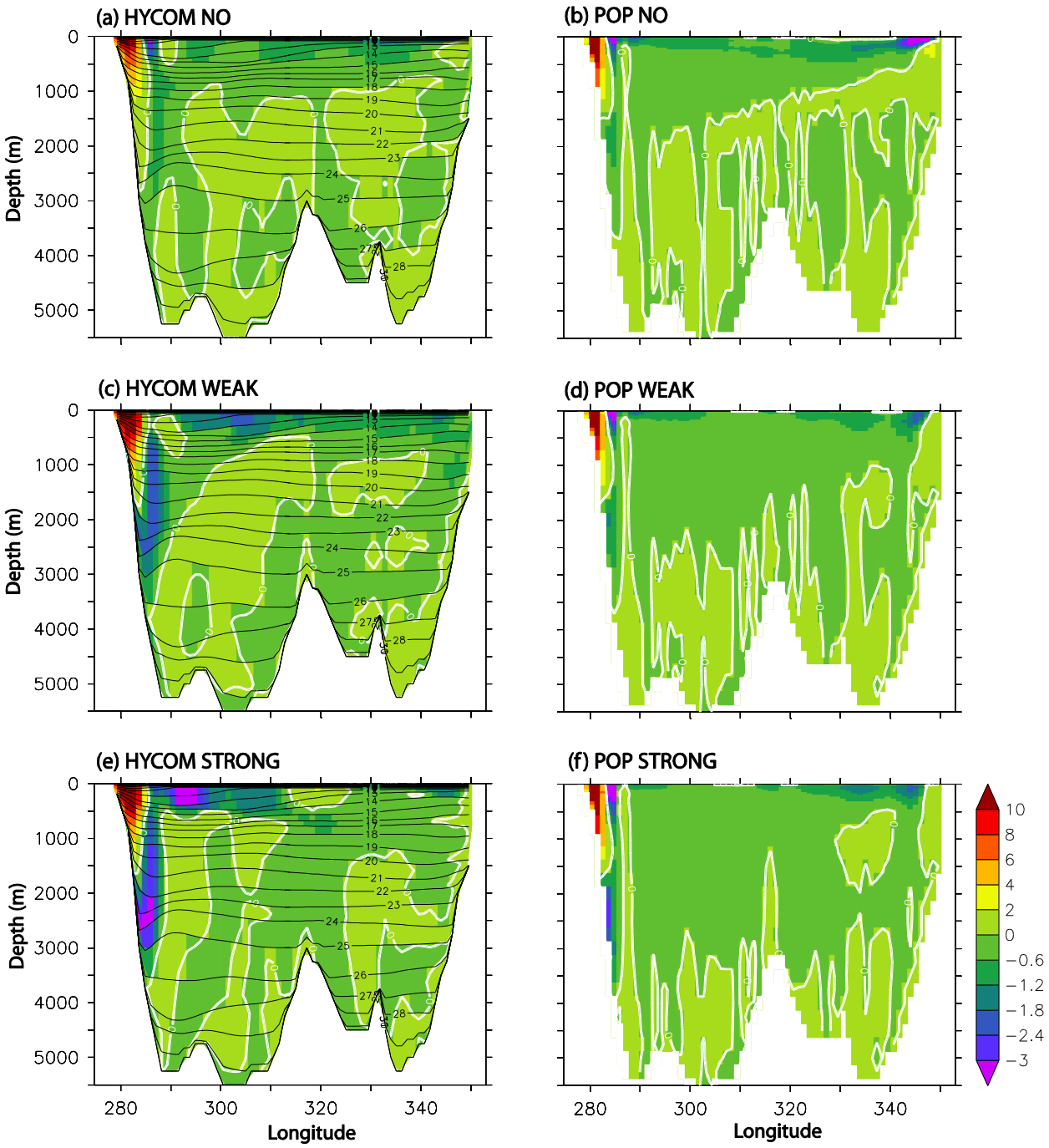
(a) HYCOM NO
(b) POP NO
(c) HYCOM WEAK
(d) POP WEAK
(e) HYCOM STRONG
(f) POP STRONG
Depth (m)
0
1000
2000
3000
4000
5000
280
300
320
340
Longitude
10
8
6
4
2
0
−0.6
−1.2
−1.8
−2.4
−3

Figure 4

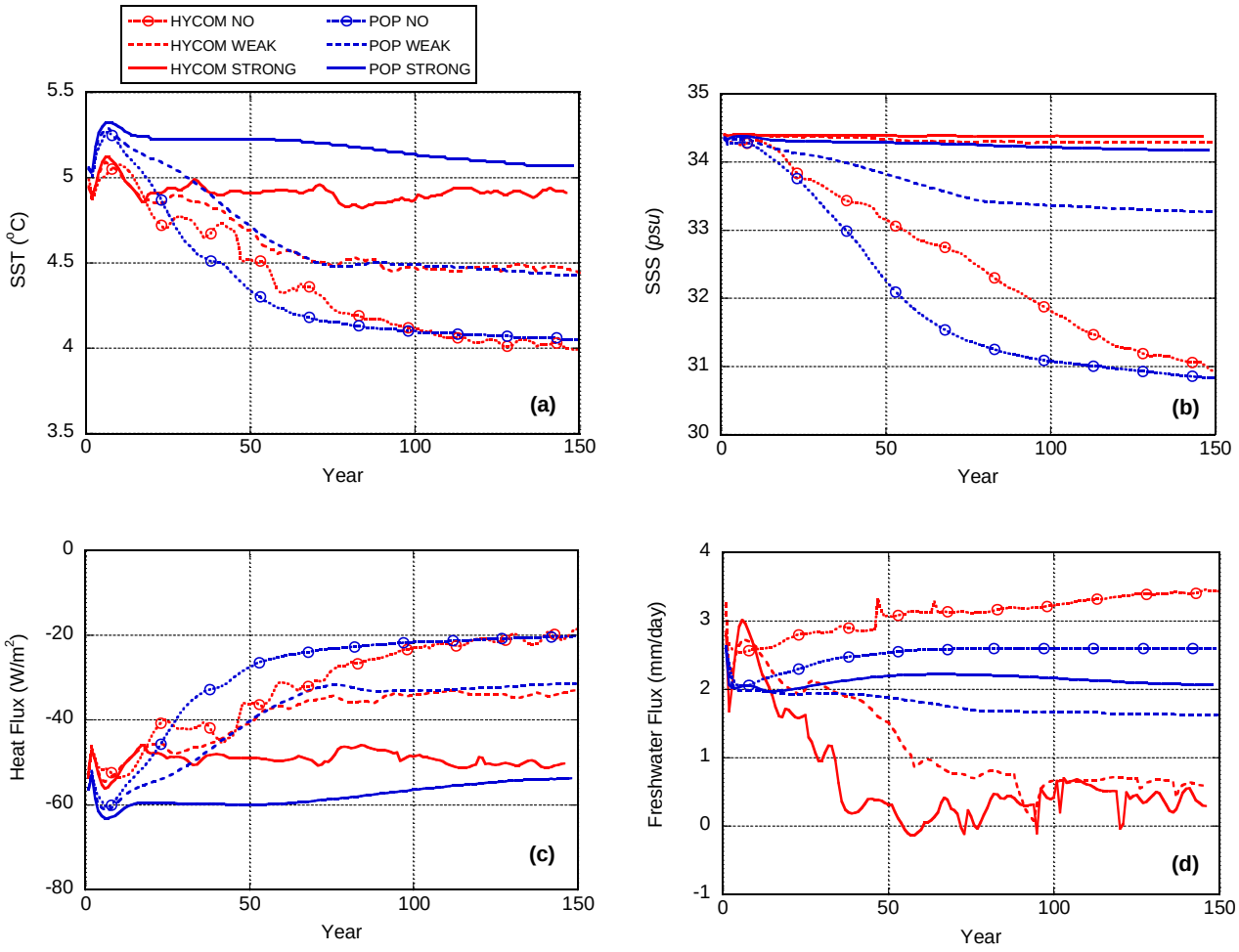
HYCOM NO
HYCOM WEAK
HYCOM STRONG
POP NO
POP WEAK
POP STRONG
SST (°C)
SSS (psu)
Heat Flux (W/m²)
Freshwater Flux (mm/day)
Year
(a)
(b)
(c)
(d)

Figure 5

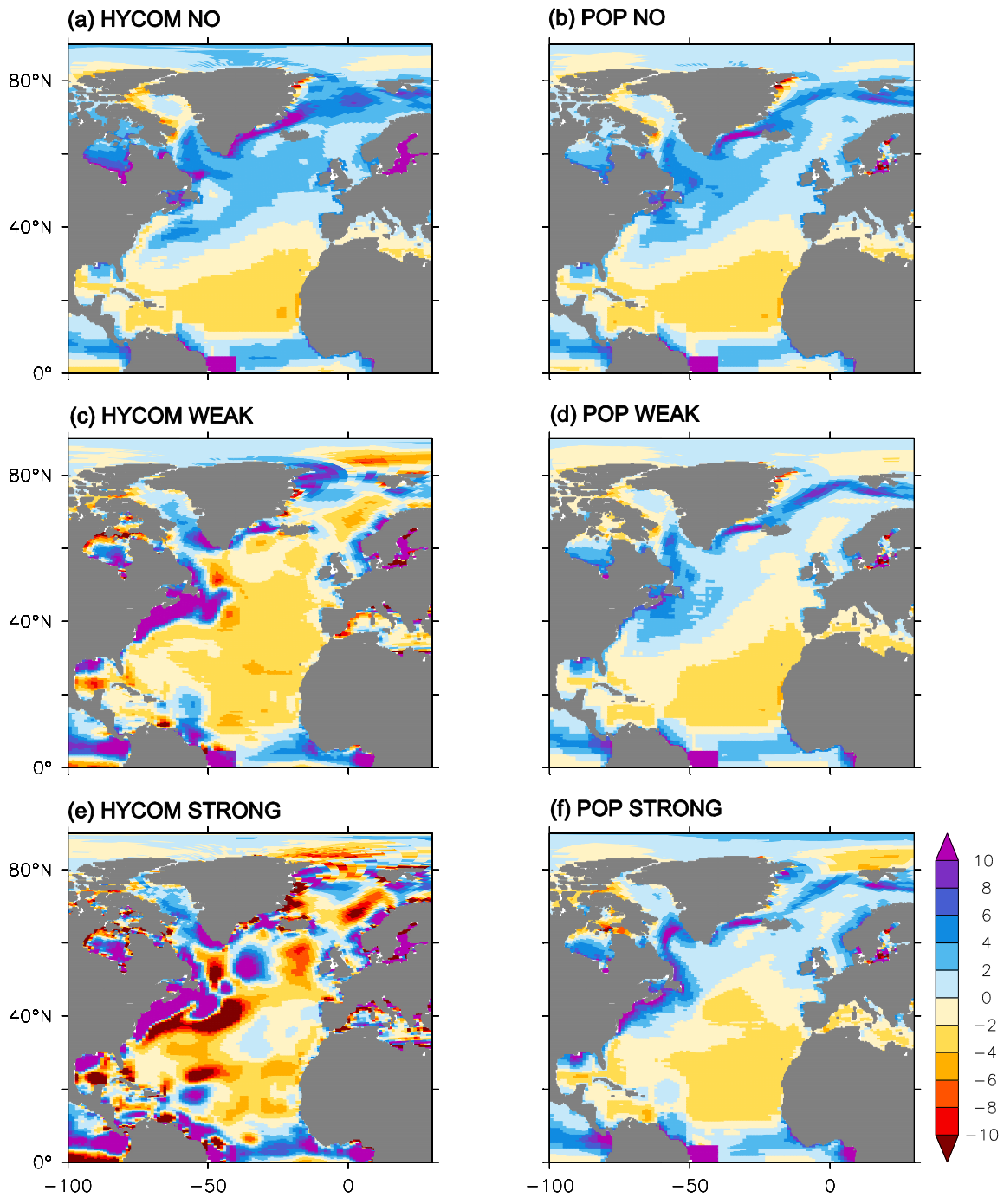
(a) HYCOM NO
(b) POP NO
(c) HYCOM WEAK
(d) POP WEAK
(e) HYCOM STRONG
(f) POP STRONG
80°N
40°N
0°
−100
−50
0
10
8
6
4
2
0
−2
−4
−6
−8
−10

Figure 6

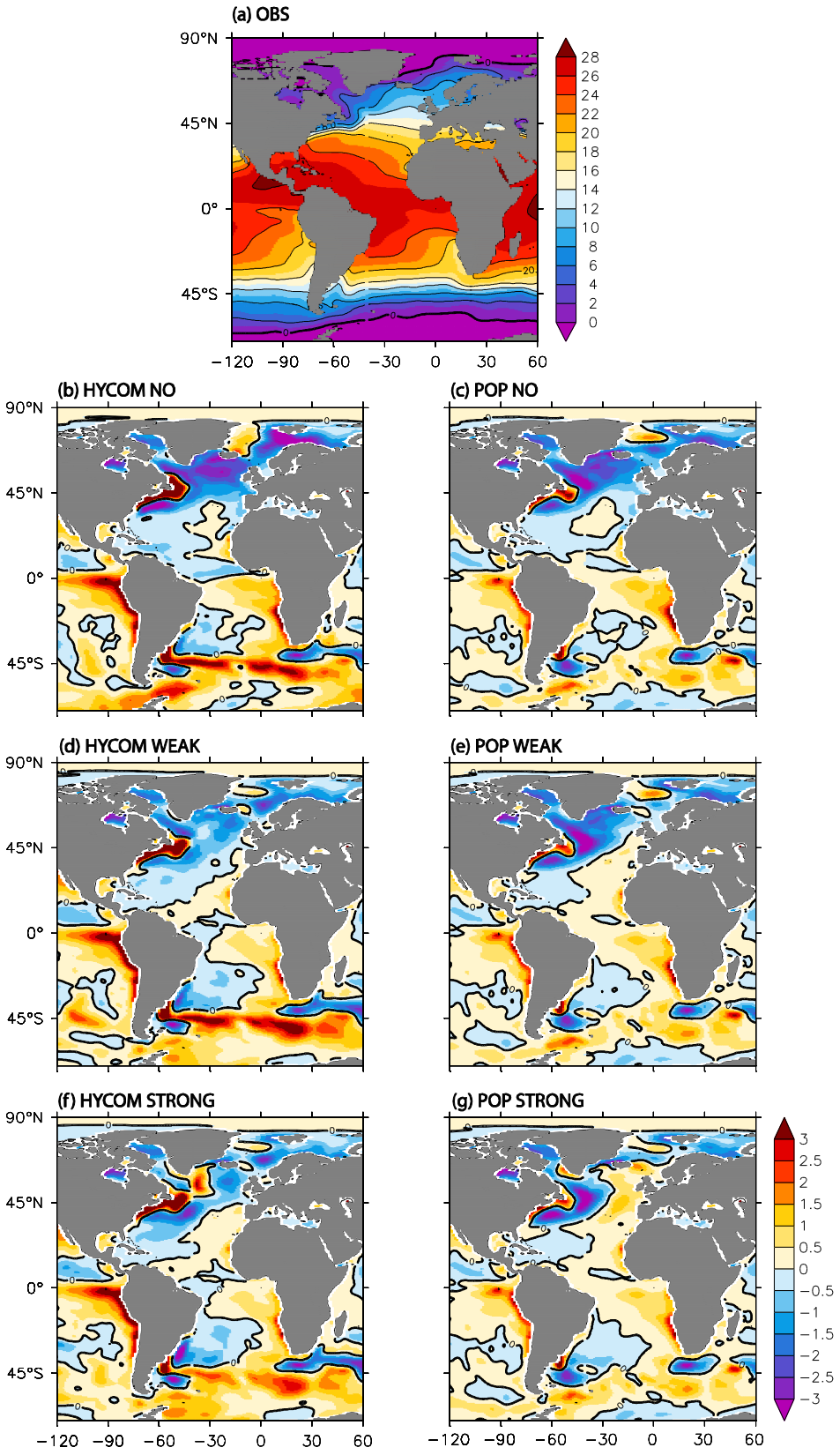
(a) OBS
90°N
45°N
0°
45°S
−120 −90 −60 −30 0 30 60
28
26
24
22
20
18
16
14
12
10
8
6
4
2
0
(b) HYCOM NO
(c) POP NO
(d) HYCOM WEAK
(e) POP WEAK
(f) HYCOM STRONG
(g) POP STRONG
3
2.5
2
1.5
1
0.5
0
−0.5
−1
−1.5
−2
−2.5
−3

Figure 7

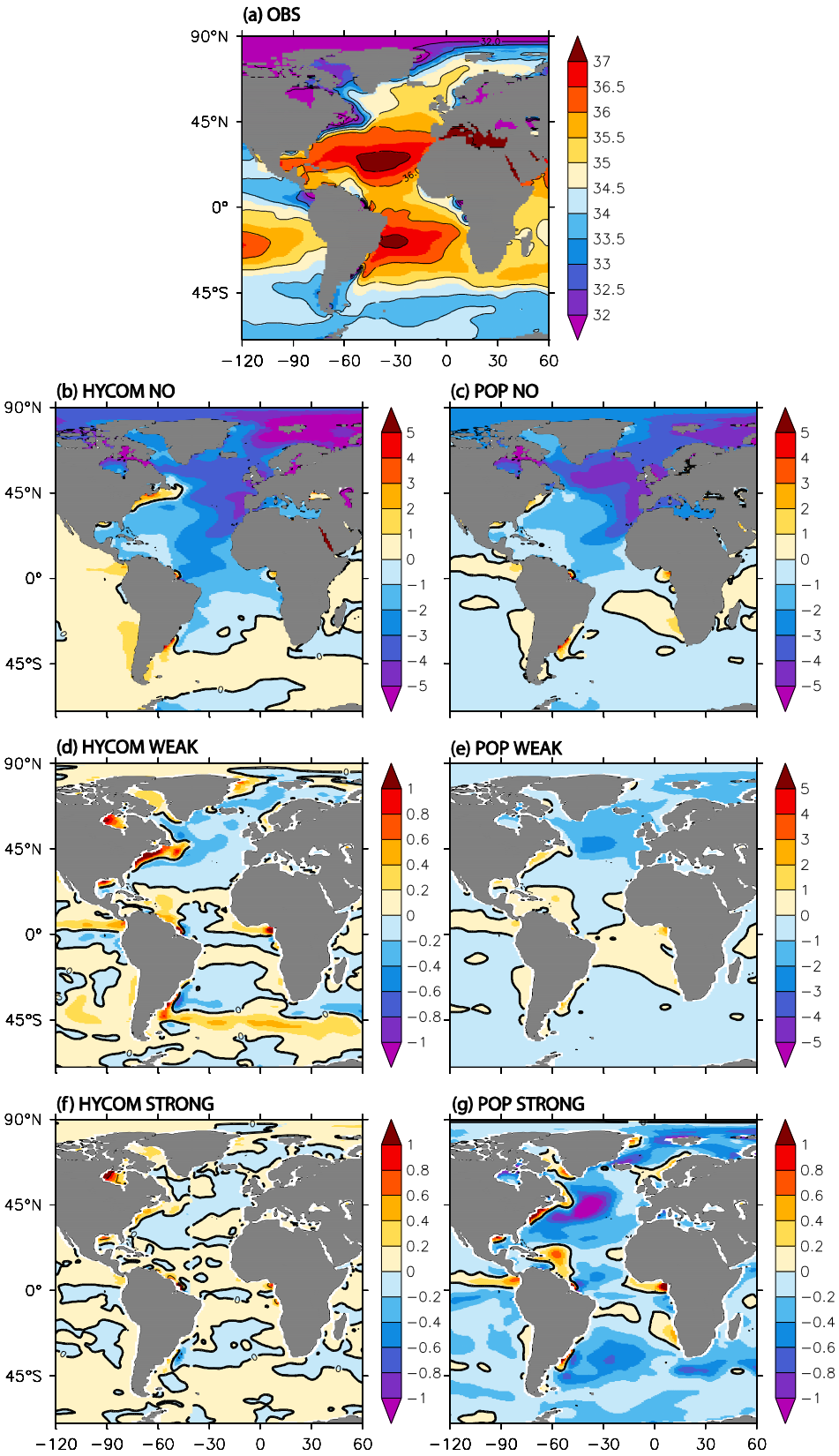
(a) OBS
90°N
45°N
0°
45°S
−120 −90 −60 −30 0 30 60
37
36.5
36
35.5
35
34.5
34
33.5
33
32.5
32
(b) HYCOM NO
(c) POP NO
5 4 3 2 1 0 −1 −2 −3 −4 −5
(d) HYCOM WEAK
(e) POP WEAK
1 0.8 0.6 0.4 0.2 0 −0.2 −0.4 −0.6 −0.8 −1
(f) HYCOM STRONG
(g) POP STRONG

Figure 8

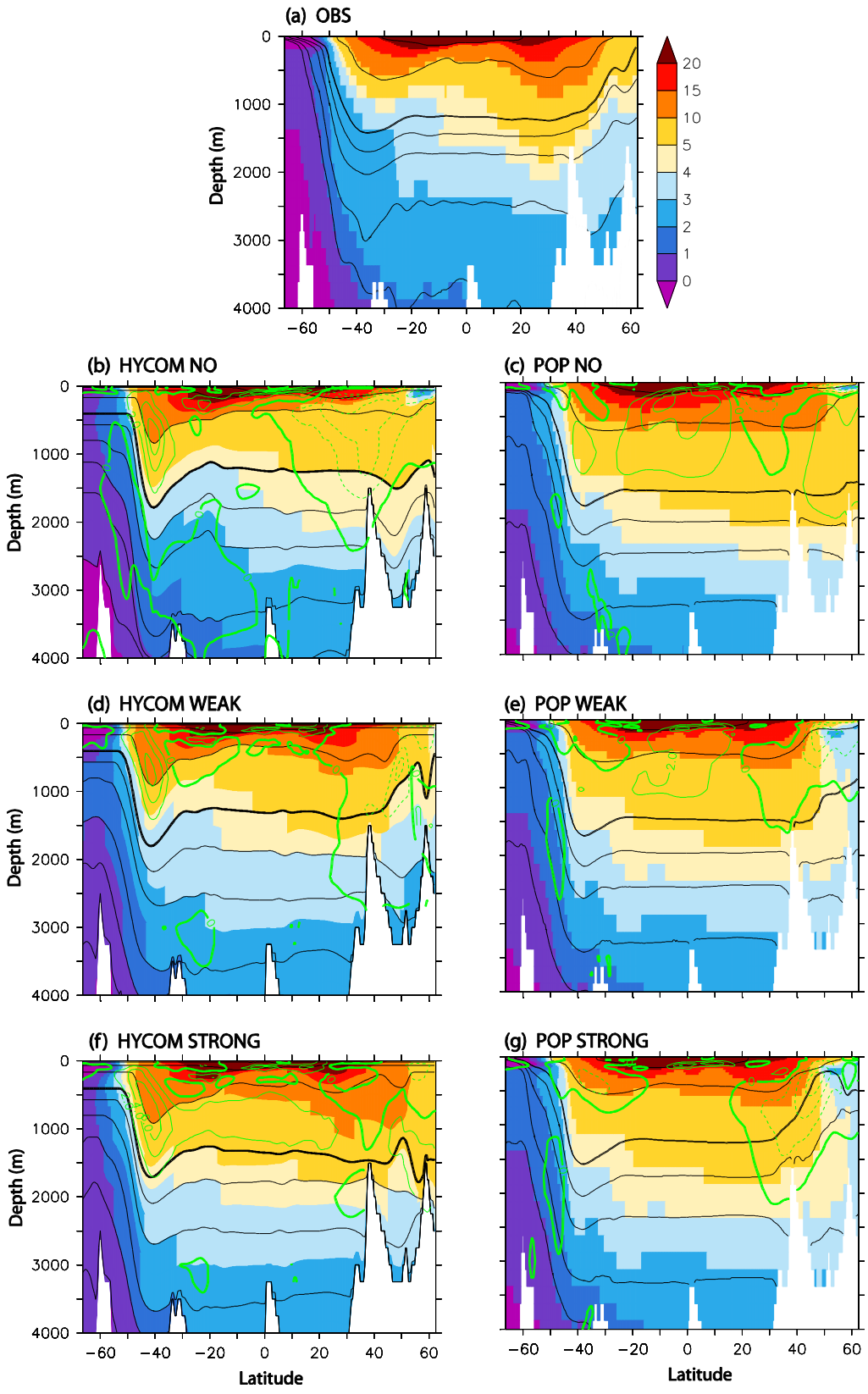
(a) OBS
(b) HYCOM NO
(c) POP NO
(d) HYCOM WEAK
(e) POP WEAK
(f) HYCOM STRONG
(g) POP STRONG
Depth (m)
Latitude
0
1000
2000
3000
4000
−60
−40
−20
0
20
40
60
20
15
10
5
4
3
2
1
0

Figure 9

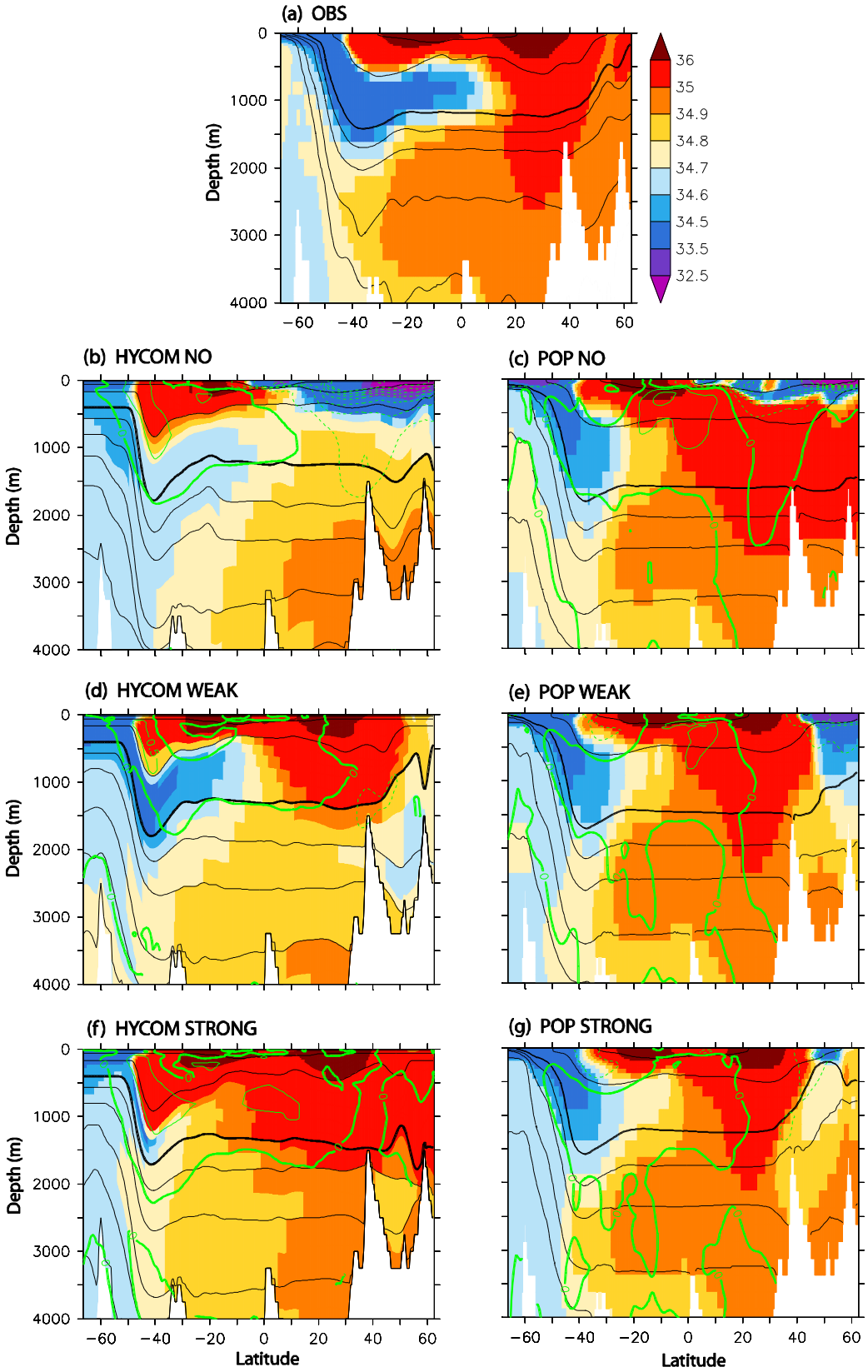
(a) OBS
(b) HYCOM NO
(c) POP NO
(d) HYCOM WEAK
(e) POP WEAK
(f) HYCOM STRONG
(g) POP STRONG
Depth (m)
Latitude
0
1000
2000
3000
4000
−60
−40
−20
0
20
40
60
36
35
34.9
34.8
34.7
34.6
34.5
33.5
32.5

Figure 10

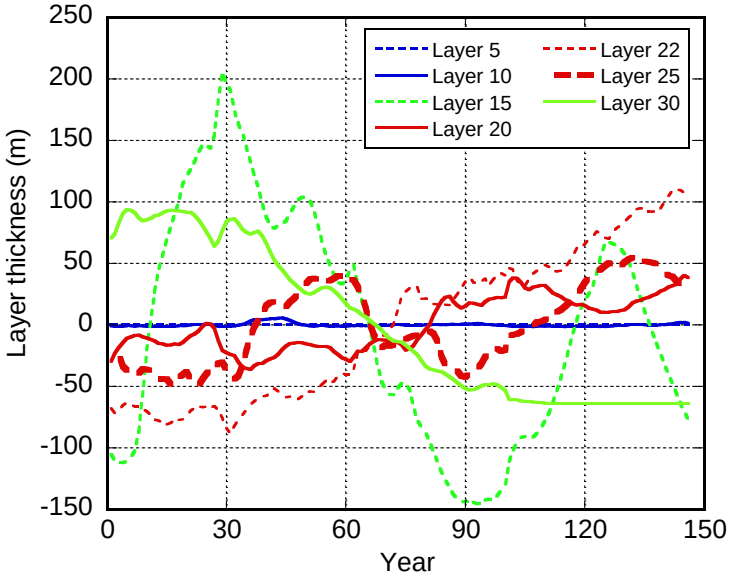
Layer 5
Layer 10
Layer 15
Layer 20
Layer 22
Layer 25
Layer 30
Layer thickness (m)
Year
250
200
150
100
50
0
-50
-100
-150
0
30
60
90
120
150

Figure 11

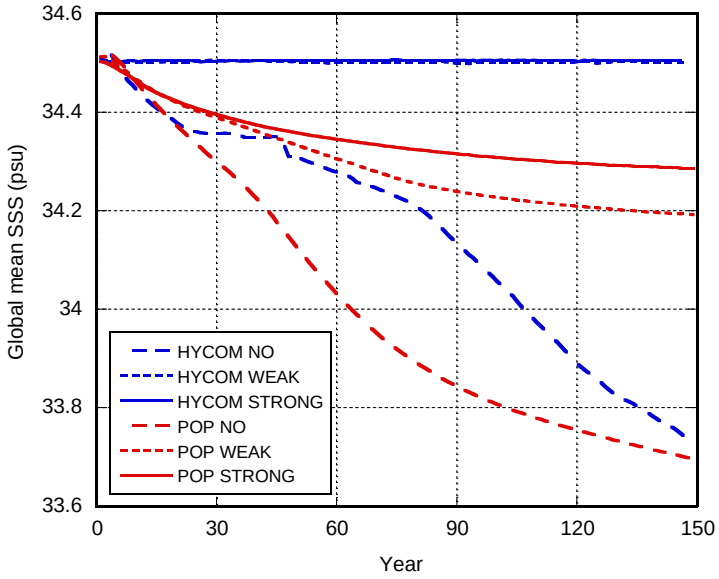
34.6
34.4
34.2
34
33.8
33.6
Global mean SSS (psu)
0
30
60
90
120
150
Year
HYCOM NO
HYCOM WEAK
HYCOM STRONG
POP NO
POP WEAK
POP STRONG

Figure 12